remote sensing

MDPI

Article

A Sparse SAR Imaging Method Based on Multiple Measurement Vectors Model

Dongyang Ao, Rui Wang *, Cheng Hu and Yuanhao Li

Beijing Key Laboratory of Embedded Real-Time Information Processing Technology, School of Information and Electronics, Beijing Institute of Technology, Beijing 100081, China; aodongyang@foxmail.com (D.A.); cchchb@163.com (C.H.); lyh.900101@163.com (Y.L.)

* Correspondence: bit.wangrui@gmail.com; Tel.: +86-10-6891-8127

Academic Editors: Francesco Soldovieri, Raffaele Persico, Xiaofeng Li and Prasad S. Thenkabail

Received: 12 October 2016; Accepted: 11 March 2017; Published: 22 March 2017

Abstract: In recent decades, compressive sensing (CS) is a popular theory for studying the inverse problem, and has been widely used in synthetic aperture radar (SAR) image processing. However, the computation complexity of CS-based methods limits its wide applications in SAR imaging. In this paper, we propose a novel sparse SAR imaging method using the Multiple Measurement Vectors model to reduce the computation cost and enhance the imaging result. Based on using the structure information and the matched filter processing, the new CS-SAR imaging method can be applied to high-quality and high-resolution imaging under sub-Nyquist rate sampling with the advantages of saving the computational cost substantially both in time and memory. The results of simulations and real SAR data experiments suggest that the proposed method can realize SAR imaging effectively and efficiently.

Keywords: SAR; compressive sensing; multiple measurement vector

1. Introduction

SAR imaging is an important observation technique in remote sensing field and has the capability of realizing all-weather and all-time observation, which can be applied in disaster detection, global mapping and environmental protection [1]. The algorithms of SAR imaging are one of the most concerning issues in the signal processing field nowadays. However, with the development of the radar technology, radar systems are confronted with many limitations, such as limited bandwidth, high-speed sampling rate and large storage space. Conventional SAR imaging algorithms cannot satisfy the requirements of modern engineering applications [1]. In order to keep up with the development of radar hardware, new imaging methods have been proposed on the basis of special characteristics of the microwave imaging theory.

Many methods have been proposed for improving SAR imaging framework with respect to both the processing speed and the image quality. They can be segmented into matched filtering methods and regularization methods [2]. As for matched filter algorithms, many commonly used SAR image processing methods can be classified, such as Range-Doppler, Chirp Scaling and $\omega - K$ algorithm. As for regularization methods, the most popular one is the CS-based SAR imaging algorithms, which assume that most imaging scenes are sparse as they often contain little scatter. The CS-based SAR imaging systems can break the Nyquist law and have potential advantages in reducing system sampling rate, improving image quality, reducing measurement burden, increasing the scope of the survey scene, and improving anti-jamming performance [3]. Thus, it becomes a research front in microwave imaging field. In [4], a radar imaging method based on CS was proposed. It could surpass the limitation of the matched filter and the bandwidth of the A/D (Analog to Digital) of the data collector in the receiver. In [5], researchers have improved the SAR imaging mode and

decreased the azimuth samples by using the CS technique. In [6], SAR imaging was realized by two one-dimensional inverse-transform issues and the CS technology can be used separately in the two dimensions. CS technology was also used in tomography in [7]. Meanwhile, CS theory has been used in 3D-SAR imaging [8]. Bu H. et al. [9,10] have applied the CS theory into practical SAR imaging, such as RADARSAT-1 and airborne SAR data, and provided new CS-SAR images with a series of advantages, such as high resolution and low side-lobes.

However, little attention has been devoted to the application of the CS theory in fast SAR imaging systems, as well as the combination of the CS technology and the traditional radar imaging algorithms. Most CS-based SAR methods merely consider the SAR imaging as an inverse problem and use the idea of matrix to solve the problem [11,12]. As a result, these methods have the problem of large computational cost and complicated structure. There is no special optimization of SAR imaging. In this paper, we introduce CS technologies into the traditional SAR algorithm. Compared with conventional SAR imaging algorithms and the data collector systems, the proposed system has the following innovations: (1) Introduce the CS theory to the conventional SAR algorithm. We have designed a novel imaging algorithm that combines the CS methods with the Back-Projection algorithm. (2) Improve the CS-SAR imaging framework based on the multiple measurement vector (MMV) models. MMV problems derive from many applications areas, such as magnetoencephalography, which is a modality for imaging the brain [13]. Similar conceptions were also developed in the context of array processing [14,15] equalization of sparse communication channels [16,17], and more recently line spectrum denoising [18] and cognitive radio communications [19]. In this paper, we want to incorporate this fast growing field into SAR imaging applications. The main topic of this paper is how to exploit MMV to reduce the number of measurements needed to faithfully represent it and make the results reliable. The proposed method is superior to the SMV-based CS algorithm, in both time consumed and reconstruction precision. Especially in the range compression, it has shortened the processing time and can further reduce the sampling data compared with the existing CS imaging algorithms.

This paper is organized as follows. Section 2 demonstrates the details of the conventional SAR imaging algorithms and SAR signal models. In Sections 3 and 4, we deeply explain the CS technology, including the algorithm and the MMV model. Simulation experiments and real data experiments based on the case of the step-frequency radar are given. In Section 5, the advantages of the proposed method are discussed. Finally, Section 6 concludes this paper and gives research perspectives.

2. CS-SAR Signal Model Based on Single Measure Vector Model

In this section, the basic knowledge of traditional SAR focusing method and CS-SAR imaging framework in the Single Measurement Vector (SMV) model are introduced. To study the SAR signal model in a convenient way, we assume that the SAR system analyzed in the paper obeys the following three conditions: (1) only single bounces are considered; (2) electromagnetic wave propagates under plane wave approximation; and (3) the SAR mode is spotlighted and circular. The circular SAR is a popular SAR system in remote sensing and it can provide full aspect coverage on interesting scenes in one run [20]. Besides, the transmit signal model is set to work in the stepped frequency mode. Compared with the LFM (Linear Frequency Modulation) waveform, stepped frequency waveforms [21,22] can easily realize ultra-wide bandwidth using only a simple hardware.

2.1. Spotlight-SAR Signal Model

The geometric configuration of a spotlighted monostatic circular SAR is shown in Figure 1.

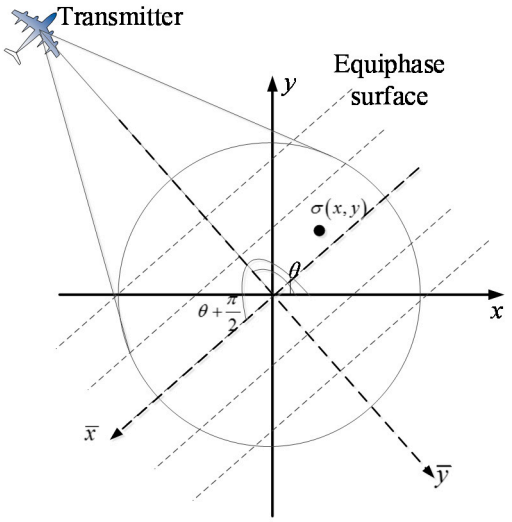

Figure 1. Geometric configuration of a monostatic SAR (synthetic aperture radar).

In Figure 1, x, y stands for the coordination of scene, while $\overline{x}$, $\overline{y}$ is the local coordination of a particular time when the transmitter moves into a position where the angle is θ under the $x-y$ coordination. Therefore, the relationship between the local and the global system is:

$$\begin{cases} \overline{x} = x\cos\left(\theta+\frac{\pi}{2}\right)+y\sin\left(\theta+\frac{\pi}{2}\right) = -x\sin\theta+y\cos\theta \\ \overline{y} = -x\sin\left(\theta+\frac{\pi}{2}\right)+y\cos\left(\theta+\frac{\pi}{2}\right) = -x\cos\theta-y\sin\theta \end{cases} \tag{1}$$

The echo signal received by the receiver can be written as:

$$s(t) = \iint \sigma(x,y)A(t-\tau(\overline{y}))dxdy \tag{2}$$

where $\tau(\overline{y}) = 2(R_0+\overline{y}\cos\psi)/c$, R_0 is the radius of the radar motion circle, $A(t)$ is the transmit signal and $\sigma(x,y)$ is the scattering coefficient of the target (x,y). Substituting Equation (1) into Equation (2), we can get:

$$s(t) = \iint \sigma(x,y)s\left(t-\frac{2(R_0-x\cos\theta-y\cos\theta)}{c}\right)dxdy \tag{3}$$

In this paper, the step frequency signal is used as the transmit signal. The step frequency signal consists of a series of single frequencies and its formula can be set as $A(t) = \exp(j\omega_i t)$, $\omega_i = \omega_0 + i\Delta\omega$, $i = 1,2,\cdots,n$, where ω_0 is the start frequency and $\Delta\omega$ is the frequency interval. For convenience, we just consider the situation of a single point frequency ω, rewriting Equation (3):

$$s(t) = \iint \sigma(x,y)\exp\left[j\omega\left(t-\frac{2(R_0-x\cos\theta-y\sin\theta)}{c}\right)\right]dxdy \tag{4}$$

After the down-conversion and the phase compensation, Equation (4) can be written as a function of θ and ω:

$$S(\omega,\theta) = \iint \sigma(x,y)\exp\left[j\frac{2\omega}{c}(x\cos\theta+y\sin\theta)\right]dxdy \tag{5}$$

Hereto, the echo signal model of the monostatic circular SAR is obtained. Equation (5) reveals the relationship between the space domain (x,y) and the signal domain (ω,θ), which is the foundation of SAR imaging. Next, the imaging algorithm is discussed to extract scene information from the collected data.

2.2. Back-Projection Imaging Algorithm

BP imaging algorithm is a typical SAR processing method [23] and has been widely used in practical applications. For a point (x_0, y_0) in the final SAR image, its pixel value $I(x_0, y_0)$ in the BP method can be written as:

$$I(x_0, y_0) = \int_{\theta_1}^{\theta_2} \int_{\omega_c - \frac{B}{2}}^{\omega_c + \frac{B}{2}} S(\omega, \theta) \exp\left[-j\frac{2\omega}{c}(x_0 \cos\theta + y_0 \sin\theta)\right] d\omega d\theta \tag{6}$$

where θ_1 and θ_2 are the angle range of radar movement, ω_c is the carrier frequency and B is the bandwidth of the stepped frequency signal. Equation (6) has the format of the double integral, so we simplify it by using integration by parts. The first integration is considered as the 1-D Fourier transform value at $2(x_0 \cos\theta + y_0 \sin\theta)/c$. Rewriting Equation (6):

$$I(x_0, y_0) = \int_{\theta_1}^{\theta_2} IFFT\left\{S\left(\frac{2}{c}(x_0 \cos\theta + y_0 \sin\theta)\right)\right\} \exp\left(j\frac{2\omega_c}{c}(x_0 \cos\theta + y_0 \sin\theta)\right) d\theta \tag{7}$$

Usually, SAR imaging is divided into range direction and azimuth direction, which can be revealed by Equation (7). $IFFT\{S\}$ is the Inverse Fast Fourier Transform (IFFT) to complete the range direction compression for the stepped frequency signal. The azimuth direction processing is conducted in the integration of θ. The computation speed in Equation (7) is faster than the double integration in Equation (6) because the 2-D problem is produced in two 1-D problems and the range direction compression is done by IFFT, which is a fast way to do Fourier transform. The details of the BP algorithm are summarized as follows.

(1) Data acquisition: Sampling the signal received by the receiver and down-conversion.
(2) Range direction compression: To accelerate the processing speed, the IFFT operation is utilized.
(3) Determining the radar position and the scene location: Using the motion trajectory of the SAR platform, phase of every PRT signal is obtained to compensate the impact of wave propagation.
(4) Azimuth direction compression: The second integration is computed by employing the result of Step 3.

2.3. CS-Theory Based on Single Measurement Vector

As for a SAR signal model in matrix format, it is written as:

$$\mathbf{Y}_{M\times 1} = \mathbf{\Phi}_{M\times N}\mathbf{X}_{N\times 1} + \mathrm{N}_{M\times 1} \tag{8}$$

where $\mathbf{Y}$ is the measurement, $\mathbf{N}$ is the noise vector, $\mathbf{\Phi}$ is the sensing matrix and the subscript indicates the number of rows and columns of the matrix. With the matrix format, the SAR imaging becomes an inverse problem of how to recover the unknown variable $\mathbf{X}$ from the measurement $\mathbf{Y}$. The most general way to get the estimation of $\mathbf{X}$ is the least squares method:

$$\hat{\mathbf{X}} = \left(\mathbf{\Phi}^H\mathbf{\Phi}\right)^{-1}\mathbf{\Phi}^H\mathbf{Y} \tag{9}$$

However, the inverse of $\mathbf{\Phi}^H\mathbf{\Phi}$ is always hard to calculate. Multiplying $\mathbf{\Phi}^H\mathbf{\Phi}$ into both sides of Equation (9) is a way to avoid computing the inverse matrix. In the aspect of SAR imaging, $\mathbf{\Phi}^H\mathbf{\Phi}$ refers to the matched filter result and is called Point Spread Function (PSF) [24]. $\mathbf{\Phi}^H\mathbf{\Phi}$ is defined by the transmit signal, and has the concept of resolution which has relation with the bandwidth. This method is only an approximation method and cannot get the exact result of $\mathbf{X}$.

Fortunately, CS theory can recover **X** exactly. To solve an undetermined problem, prior information is needed. Here, the prior information is the sparsity. The sparsity of **X** means that most of elements in **X** are zeros or their magnitudes are very small [25]. In remote sensing, there are many scenes with only a few targets. For example, ships in the ocean and strong targets in a large scale site [9]. In this paper, non-sparse targets will not be discussed.

Commonly, the recovery problem is converted to a P_0 programming problem, which is defined as:

$$P_0 : \min_{\mathbf{X}\in\mathbb{R}^N} \|\mathbf{X}\|_0 \quad s.t. \, \mathbf{\Phi X = Y} \tag{10}$$

where $\|\mathbf{X}\|_0$ denotes the number of non-zero elements of **X**. However, solving Equation (10) is difficult because it is an N-P hard problem. However, scientists have proven that once the sensing matrix $\mathbf{\Phi}$ satisfies the restricted isometric property (RIP), the P_0 problem has the same solution as P_1:

$$P_1 : \min_{\mathbf{X}\in\mathbb{R}^N} \|\mathbf{X}\|_1 \quad s.t. \, \mathbf{\Phi X = Y} \tag{11}$$

where $\|\mathbf{X}\|_1$ represents the l_1 norm of **X**. A matrix $\mathbf{\Phi}$ is said to satisfy the RIP of order K if there exists a constant $\delta_K \in (0,1)$ such that

$$(1-\delta_k)\|\mathbf{X}\|^2 \leq \|\mathbf{\Phi X}\|^2 \leq (1+\delta_k)\|\mathbf{X}\|^2 \tag{12}$$

holds for all $\|\mathbf{X}\|_0 \leq K$. This is the necessary and sufficient condition for changing compressive sensing to P_1 problem. To make the sensing matrix reach RIP condition, there are three common ways to construct the matrix: by the random matrix, by the stochastic structure matrix and by the deterministic matrix [26]. Considering our tasks and the signal model, we choose the random matrix way because the random sampled Fourier dictionary is commonly used and its RIP has been proven [27]. In this section, we will discuss the combination of CS theory and SAR imaging.

The stepped frequency waveform is

$$s(m,t) = rect\left(\frac{t}{T_p}\right)\exp[j2\pi f_c(m)t] \tag{13}$$

where $m = 1, 2, \cdots, M$ denotes the mth pulse in a sequence; and M is the total sampling number of a transmitted signal. $rect\left(t/T_p\right)$ demonstrates the continuum time and T_p is the window width. $f_c(m)$ is the carry frequency in the mth pulse and varies linearly in time:

$$f_c(m) = f_c + m\Delta f, \; m = 1, 2, \cdots, M \tag{14}$$

where f_c is the start frequency and Δf is the frequency step length. Using Equation (13) to rewrite Equation (5):

$$S(f_m, \theta_t) = \iint \sigma(x,y)\exp\left[-j\frac{4\pi f_m R_t}{c}\right]dxdy \tag{15}$$

where $R_t = x\cos\theta_t + y\sin\theta_t$. When the IFFT operation takes place in Equation (14), the result becomes the range image, whose peak position is decided by R_t where the target locates and the range resolution is related with the range of $f_c(m)$.

To apply the CS theory in SAR imaging, the integrations should be converted to matrix format. According to Equation (15), its discretization is

$$s(m,n) = \sum_{i=1}^{X}\sum_{j=1}^{Y}\sigma(i,j)\exp\left[-j\frac{4\pi f_m R(i,j,n)}{c}\right] \tag{16}$$

where i and j are the positions of the targets, m is the sampled frequency and n denotes the PRT number. $R(i,j,n)$ is the distance from target (i,j) to radar in the nth PRT. In order to change Equation (16) to matrix format, we denote that:

$$\mathbf{Y} = [s(1,1), s(1,2), \cdots, s(1,N), s(2,1), s(2,2), \cdots, s(2,N), \cdots, s(M,1), \cdots s(M,N)]^T \quad (17)$$

$$\mathbf{X} = [\sigma(1,1), \sigma(1,2), \cdots \sigma(1,Y), \cdots, \sigma(X,1), \sigma(X,2), \cdots \sigma(X,Y)]^T \quad (18)$$

Since the observed data are less than the number of the scene targets, we have $MN < XY$. We firstly define that:

$$\phi(m,n,i,j) = \exp\left[-j\frac{4\pi(f_c + \Delta f m)R(i,j,n)}{c}\right] \quad (19)$$

Having Equation (19), the basic unit of $\mathbf{\Phi}$ is

$$\Phi(m,n) = [\phi(m,n,1,1), \phi(m,n,1,2), \cdots, \phi(m,n,1,Y), \cdots, \phi(m,n,X,1), \cdots, \phi(m,n,X,Y)] \quad (20)$$

Thus, the $\mathbf{\Phi}$ can be defined as:

$$\mathbf{\Phi} = [\Phi(1,1), \Phi(1,2), \cdots, \Phi(1,N), \Phi(2,1), \cdots, \Phi(2,N), \cdots, \Phi(M,1), \cdots, \Phi(M,N)]^T \quad (21)$$

where $\mathbf{\Phi}$ is an $MN \times XY$ matrix. After getting the measurement vector $\mathbf{Y}$, the result vector $\mathbf{X}$ and the sensing matrix $\mathbf{\Phi}$, Equation (16) is written as:

$$\mathbf{Y} == \begin{bmatrix} s(1,1) \\ s(1,2) \\ \vdots \\ s(1,N) \\ s(2,1) \\ s(2,2) \\ \vdots \\ s(2,N) \\ \vdots \\ s(M,1) \\ s(M,2) \\ \vdots \\ s(M,N) \end{bmatrix} = \mathbf{\Phi} + \mathbf{N} = \begin{bmatrix} \Phi(1,1) \\ \Phi(1,2) \\ \vdots \\ \Phi(1,N) \\ \Phi(2,1) \\ \Phi(2,2) \\ \vdots \\ \Phi(2,N) \\ \vdots \\ \Phi(M,1) \\ \Phi(M,2) \\ \vdots \\ \Phi(M,N) \end{bmatrix} \begin{bmatrix} \sigma(1,1) \\ \sigma(1,2) \\ \vdots \\ \sigma(1,Y) \\ \vdots \\ \sigma(X,1) \\ \sigma(X,2) \\ \vdots \\ \sigma(X,Y) \end{bmatrix} + \mathbf{N} \quad (22)$$

Equation (22) is an equation connecting target scene and raw data. Through computing the equation, the final SAR image can be recovered at a time. The model of Equation (22) is called single measurement vector model (SMV) because the unknown SAR image is regarded as a one-dimensional vector and the radar observation is represented in one equation. From the above description, the SAR-SMV model establishment process is presented.

3. SAR Imaging Based on Multiple Measurement Vector Model

The imaging methods based on SMV have been discussed for a long time [25]. However, the SMV model has large scale matrixes and high computational complexity, which will consume many resources for both computing and storage. For example, the size of $\mathbf{\Phi}$ is $MN \times XY$, which is large-scale. The entire system was designed to convert the SAR signal model into a matrix without adding any optimization for SAR imaging. The whole process is the same, even with other problems.

Consequently, only small-scale imaging tasks are suitable to apply the SMV or a powerful computer is required. In order to overcome these shortcomings, a new CS-based SAR focusing method is proposed.

In traditional SAR imaging algorithms, the raw data are usually processed in two direction dimensions: range direction and azimuth direction. In this section, we take advantages of CS theory to improve the performance of BP algorithm and make a compromise between the resolution and the computation.

3.1. Structured CS Model—Multiple Measurement Vectors

CS-SAR methods in SMV usually focus on the construction of the measurement matrix $\mathbf{\Phi}$ and the sparsity of unsolved signal $\mathbf{X}$. However, little attention has been paid to structure features of the SAR imaging. For a radar system, the transmit waveform is uniform. In other words, every observation equation shares a same sensing matrix. Based on this feature, a new CS-SAR framework combining the traditional SAR algorithm and the structured CS model is proposed.

The first structure information that has been considered within the CS framework has been that of multiple measurement vectors (MMV) [28]. Unlike trying to recover a single sparse vector x like SMV, the MMV model is used to recover a set of vectors, which are the columns of a matrix $\mathbf{X}$. The structure information in MMV is that each column of the unsolved matrix $\mathbf{X}$ is K-sparse, and the nonzero elements occur on a common location set.

Consider L length N discrete time signal which is denoted as a $N \times L$ matrix $\mathbf{X} = [x_1, x_2, \cdots, x_L]$. The M linear measurements of $\mathbf{X}$ with noise model can be expressed in matrix form:

$$\mathbf{Y}_{M\times L} = \mathbf{\Phi}_{M\times N}\mathbf{X}_{N\times L} + \mathrm{N}_{M\times L} \tag{23}$$

where $\mathbf{Y} = [y_1, y_2, \cdots, y_L]$ is the measurement matrix, whose rows are the data in L observation, $\mathbf{N}$ is the noise vector, and $\mathbf{\Phi}$ is the sensing matrix, which is familiar with the SMV model. The difference is that the unsolved parameters and measurement data in MMV are stored in an $N \times L$ matrix $\mathbf{X}$ and a $M \times L$ matrix $\mathbf{Y}$, respectively. Once the MMV changes to a normal inverse problem, we can apply any CS method to recover x_i. However, because of the basic assumption of MMV, all vectors have a common support and are K-sparse, we expect intuitively to improve the recovery ability by exploiting this structure information. The enhanced result is guaranteed by the following necessary and sufficient uniqueness condition [29]:

Theorem 1. *A necessary and sufficient condition for the measurements* $\mathbf{Y} = \mathbf{\Phi X}$ *to uniquely determine the jointly sparse matrix* $\mathbf{X}$ *is that*

$$|supp(\mathbf{X})| < \frac{spark(\mathbf{\Phi}) - 1 + rank(\mathbf{X})}{2} \tag{24}$$

A direct consequence of Theorem 1 is that matrices $\mathbf{X}$ with larger rank can be recovered from fewer measurements. When $rank(\mathbf{X}) = K$ and $spark(\mathbf{X})$ takes on its largest possible value equal to $M + 1$, the condition in Equation (24) becomes $M > K + 1$. Thus, in the best case, each signal requires only $K + 1$ measurements to ensure uniqueness. However, the minimum measurements for SMV are $2K$, which is much larger than the MMV. Thus, the MMV can recovery signals with fewer data. This is the theory foundation of MMV. Referring to [25], more details can be obtained.

Next, we will apply the MMV model to the SAR imaging framework. Enlightened by the BP algorithm, the SAR-MMV imaging is decoupled into the range direction and the azimuth direction. As for the range direction processing, the CS-MMV model can be used to improve the resolution and reduce the date sampling rate. The signal model of the radar sampling in the range direction is:

$$F(f) = \int \sigma(r) e^{-j\frac{4\pi f}{c}r} dr \tag{25}$$

After the discretization, we have:

$$F(f_i) = \sum \sigma(n) e^{-j\frac{4f_i}{c}n} \tag{26}$$

Its matrix format is:

$$\begin{bmatrix} F_1 \\ F_2 \\ \vdots \\ F_M \end{bmatrix} = \begin{bmatrix} e^{-j\frac{4\pi f_1}{c}r_1} & e^{-j\frac{4\pi f_1}{c}r_2} & \cdots & e^{-j\frac{4\pi f_1}{c}r_{n-1}} & e^{-j\frac{4\pi f_1}{c}r_N} \\ e^{-j\frac{4\pi f_2}{c}r_1} & e^{-j\frac{4\pi f_2}{c}r_2} & \cdots & e^{-j\frac{4\pi f_2}{c}r_{n-1}} & e^{-j\frac{4\pi f_2}{c}r_N} \\ \vdots & \vdots & \vdots & \vdots & \vdots \\ e^{-j\frac{4\pi f_M}{c}r_1} & e^{-j\frac{4\pi f_M}{c}r_2} & \cdots & e^{-j\frac{4\pi f_M}{c}r_{n-1}} & e^{-j\frac{4\pi f_M}{c}r_N} \end{bmatrix} \begin{bmatrix} \sigma(r_1) \\ \sigma(r_2) \\ \vdots \\ \sigma(r_{N-1}) \\ \sigma(r_N) \end{bmatrix} \tag{27}$$

Equation (26) is the measurement equation for an observation. Since all observation shares the same sensing matrix, which is the structured information in SAR applications, solving multiple observations in one matrix computation could be a good idea to accelerate the processing speed. Thus, expanding Equation (27):

$$\begin{bmatrix} F_1^{(1)} & F_1^{(2)} & & F_1^{(L)} \\ F_2^{(1)} & F_2^{(2)} & \cdots & F_2^{(L)} \\ \vdots & \vdots & & \vdots \\ F_M^{(1)} & F_M^{(2)} & & F_M^{(L)} \end{bmatrix} = \begin{bmatrix} e^{-j\frac{4\pi f_1}{c}r_1} & e^{-j\frac{4\pi f_1}{c}r_2} & \cdots & e^{-j\frac{4\pi f_1}{c}r_{n-1}} & e^{-j\frac{4\pi f_1}{c}r_N} \\ e^{-j\frac{4\pi f_2}{c}r_1} & e^{-j\frac{4\pi f_2}{c}r_2} & \cdots & e^{-j\frac{4\pi f_2}{c}r_{n-1}} & e^{-j\frac{4\pi f_2}{c}r_N} \\ \vdots & \vdots & \vdots & \vdots & \vdots \\ e^{-j\frac{4\pi f_M}{c}r_1} & e^{-j\frac{4\pi f_M}{c}r_2} & \cdots & e^{-j\frac{4\pi f_M}{c}r_{n-1}} & e^{-j\frac{4\pi f_M}{c}r_N} \end{bmatrix} \begin{bmatrix} \sigma(r_1) & \sigma(r_1) & & \sigma(r_1) \\ \sigma(r_2) & \sigma(r_2) & & \sigma(r_2) \\ \vdots & \vdots & \cdots & \vdots \\ \sigma(r_{N-1}) & \sigma(r_{N-1}) & & \sigma(r_{N-1}) \\ \sigma(r_N) & \sigma(r_N) & & \sigma(r_N) \end{bmatrix} \tag{28}$$

where $F_m^{(l)}$ is the mth frequency data of lth observation, $l = 1, 2, \cdots, L$. In order to reduce useless data, the data in the region of interest are valuable. $r_i, i = 1, 2, \cdots, N$ are distributed equally in $[R_{\min}, R_{\max}]$ with interval ΔR. In this format, the dimension of the sensing matrix $\mathbf{\Phi}$ is much smaller than before. If the compression is done by the proposed MMV method, the solution of Equation (28) can be recovered with higher resolution and fewer measurements.

Regardless of the influence of range cell migration, all azimuth sampled data have the same sparse structure. Consequently, we can use CS-MMV methods to recover the 1-D range direction imaging directly. However, in most cases, range migrations exist in every azimuth sample and the basic assumption does not satisfy all SAR imaging situations. Rather than suppose all the azimuth directions have a same sparse structure, it is assumed that the data and their adjacency in L azimuth units share one, where L is determined by the distance from radar to scene and the radar velocity and trade-off between computational complexity and representation error. Under this setting, the MMV is used multiple times to recover the whole 1-D range image. This is the first step to change the SAR imaging tasks in the MMV model.

3.2. Recovery Algorithms

Previously, the MMV model for the range compression was introduced. Here, the recovery algorithm of the MMV equation and the differences between MMV and SMV are the focus. A variety of algorithms have been proposed that exploit the joint sparsity in different ways [30]. Generally, the recovery task in CS-MMV is:

$$\hat{\mathbf{X}} = \arg \min_{\mathbf{X} \in \mathbb{R}^{N \times L}} \|\mathbf{X}\|_{0,q} + \lambda \|\mathbf{Y} - \mathbf{\Phi}\mathbf{X}\|_F^2 \tag{29}$$

where we define the norms $l_{p,q}$ for matrices as

$$\|\mathbf{X}\|_{p,q} = \left(\sum_i \|x^{(i)}\|_p^q \right)^{\frac{1}{q}} \tag{30}$$

where $x^{(i)}$ denote the ith row of $\mathbf{X}$. We assume quasi-norms when $p = 0$, $\|\mathbf{X}\|_{0,q} = |\mathrm{supp}(\mathbf{X})|$ for every q, which is equal to the $l_0 - norm$ for matrix. Different algorithms uses different forms to relax the $l_0 - norm$. Here, converting Equation (29) to

$$\hat{\mathbf{X}} = \arg \min_{\mathrm{X} \in \mathbb{R}^{N \times L}} \|\mathbf{X}\|_{p,q} + \lambda \|\mathbf{Y} - \mathbf{\Phi X}\|_F^2 \tag{31}$$

Since 2006 [31], plenty of recovery algorithms have been developed for solving the MMV problems [32,33], such as the Focal Undetermined System Solver method [34] and the Basis Pursuit method [35,36] They can be divided into two categories, the convex optimization and the greedy method. In this paper, one of the greedy algorithms, OMP (Orthogonal Matching Pursuit), is discussed because of its robustness and simplicity. It is a popular extension of matching pursuit which involves finding the "best matching" projections of multidimensional data onto the span of an over-complete dictionary [37].

In SMV models, the OMP iteratively selects the column of the sensing matrix according to their correlation with the measurements determined by inner product. As for MMV cases, the OMP has been changed. The basic idea of the MMV-OMP method is to replace the residual vector $\mathbf{r}$ by a residual matrix $\mathbf{R}$, which contains the residuals with respect to each of the measurements, and to replace the surrogate vector $\mathbf{\Phi}^H \mathbf{r}$ by the norms of the rows of $\mathbf{\Phi}^H \mathbf{R}$.

The details of MMV-OMP algorithm are shown in Algorithm 1.

Algorithm 1. MMV-OMP

Inputs: $\mathbf{Y} \in \mathbb{C}^{M \times L}$, $\mathbf{\Phi} \in \mathbb{C}^{M \times N}$, K, the sparsity of $\mathbf{X}$
Output: Row-sparse matrix $\hat{\mathrm{X}} \in \mathbb{C}^{N \times L}$
Initialization: $\mathbf{X}^0 = 0, \mathrm{R}^0 = \mathrm{Y}, \Omega^0 = \varnothing$
for $1 \le j \le K; j = j + 1$ **do**
1 **Max correlation:** $i^j = \mathrm{argmax}_i \|\mathbf{\Phi}_i^H \mathbf{R}^{j-1}\|_2$
2 **New support:** $\Omega^j = \Omega^{j-1} \cup i^j$
3 **Update Approximation:** $\mathbf{X}^j = \mathbf{\Phi}_{\Omega^j}^H \mathbf{Y}$
4 **Update Residual:** $\mathbf{R}^j = \mathbf{Y} - \mathbf{\Phi X}^j$
end for
Return $\hat{\mathrm{X}} = \mathrm{X}^K$

The MMV-OMP algorithm is a greedy method and is proposed in [38]. It has been widely used in MMV models. Due to the performances in the practical applications, the range image generated by MMV-OMP can be faster than that by the SMV model.

3.3. Two-Dimensional SAR Imaging Based on BP Method

According to Equation (26), a two-dimensional matrix whose columns are the range compression result under different apertures is obtained. The processing in Section 3.1 does not concentrate on the azimuth focusing and only generate middle results. In this section, how to use the MMV results to produce the final image is discussed.

At first, the MMV result and the traditional pulse compression result are compared. In order to remove the impact of the matrix inversion operation, the pulse compression only outputs the inner product of the reference signal and the measurement. With respect to its matrix format, we have:

$$R_{\text{pulse compression}} = \mathbf{\Phi}^H y \tag{32}$$

while the original least square result is $R_{LS} = \left(\Phi^H \Phi\right)^{-1} \Phi^H y$. With respect to the CS-MMV case, the original result is expressed as:

$$R_{CS} = \left(\Phi_\Omega^H \Phi_\Omega\right)^{-1} \Phi_\Omega^H y \tag{33}$$

where Ω is the support set defined in Section 3.1 and has nonzero element. R_{cs} is sparse and has super-resolution. However, at the same time, it is very sensitive to errors. Generally, the results of CS-based algorithms contain estimation errors. In the range direction images, the errors are not obvious and have almost no effect on presenting 1-D range profiles. However, once the errors are integrated in the azimuth direction processing, the accumulation of errors will lead to the reduced image readability.

To get a readable SAR images with MMV, the effects of errors must be reduced. Enlightened by the matched filter, a method to overcome unsuccessful reconstructions is proposed. The matched filter is widely used because of its robustness. Even when there are noises and errors, the matched filter can obtain the main information from the signal. In order to achieve the same effect, a full band sensing matrix $\mathbf{\Phi}_{full}$ is applied to compensate the sparse matrix. Consequently, the final result of MMV range direction processing is changed as:

$$R_{final} = \left(\mathbf{\Phi}_{full}{}^{H}\mathbf{\Phi}_{full}\right)R_{cs} \tag{34}$$

where $\mathbf{\Phi}_{full}$ is the sensing matrix that contains frequency atoms. The compensation term $\mathbf{\Phi}_{full}{}^{H}\mathbf{\Phi}_{full}$ is equivalent to the point spread function (PSF) in radar system. If $\mathbf{\Phi}_{full}$ equals $\mathbf{\Phi}_{\Omega}$, Equation (33) will degenerate to the matched filter method and not improve the resolution. If $\mathbf{\Phi}_{full}$ contains the whole spectrum, i.e., the PSF is the delta function, it becomes the conventional CS method again. It is found that when the intended bandwidth is much higher than the original one, the azimuth direction focusing fails. Therefore, the determination of $\mathbf{\Phi}_{full}$ is a trade-off between resolution and robustness. A $\mathbf{\Phi}_{full}$ that contains 1.5 times more frequency points than the original one has proven to be the best choice, where the frequency point is the row of the sensing matrix $\mathbf{\Phi}_{full}$ and is defined as $[\exp(-j4\pi f_i r_1/c), \exp(-j4\pi f_i r_2/c), \cdots, \exp(-j4\pi f_i r_N/c)]$. In other words, the number of rows in $\mathbf{\Phi}_{full}$ is 1.5 times the original matrix $\mathbf{\Phi}$. Only in this way will both the resolution of the range direction and the robustness be increased. Then, azimuth processing can begin.

Learning from the classical BP algorithm, the CS range direction image is used to process the azimuth direction result. In the traditional range compression, IFFT operation takes place in the baseband while the correct result of matched filter is produced in the transmit band. The results by IFFT will have an extra linear phase in the frequency domain. As a result, the 1-D range profile has a residual central phase. However, in the modified MMV method, the received signal is processed by the dictionary atoms in the transmit band. The definition of $\mathbf{\Phi}$ is the same with Equation (21). Thus, the phase compensation is no longer needed. The result from the MMV model can be directly used in azimuth processing.

Defining $R_{1D}(r, q)$ as the result after one-dimensional range compression in the MMV model, r as the range direction, and q as the order of the position of the radar, the expression of azimuth processing is as follows:

$$I(x, y) = \sum_{q=1}^{N} R_{1D}\left(\left\lfloor \frac{x\cos\theta_q + y\sin\theta_q - R_{\min}}{\Delta R} \right\rfloor, q\right) \tag{35}$$

Hereby, the final image $I(x, y)$ is obtained.

From the analyses in the previous subsections, it can be seen that the proposed new CS-SAR framework has constituted a more efficient CS-based SAR imaging method. While preserving CS features, the new method has the following exclusive advantages.

1. Lower computation cost and fewer needed data: Due to the use of the MMV model, we can recovery multiple azimuth direction samples at one time with high speed and save the memory cost.
2. High compatibility and high resolution: The MF-like azimuth processing to enhance the robust of the algorithm, which can fit most cases of SAR imaging. The improved CS-SAR method can

take the advantage of BP and CS method, and robustly produce high-resolution images using the same amount of data.

All the features make the proposed new CS-SAR method more useful and efficient.

4. Simulations and Experiments

In this section, simulations and experiments are conducted, where the SAR signal mode is stepped frequency and the frequency data are randomly sampled. In addition, the full aperture data are used to recover the test scene.

First, we conduct simulations to compare the matched filter method, the SMV model, and the MMV model in terms of the image quality, the computation cost, and the recovery speed. Second, experiments are done for proving that the suggested new CS-SAR method is a better choice for SAR imaging. The simulation parameters are shown in Table 1.

Table 1. Simulation parameters.

Carrier Frequency	10 GHz
Bandwidth	2 GHz
Frequency interval	40 MHz
Angle Range	85°–95°
Angle interval	0.1°
Initial Distance	30,000 m

4.1. Simulations

In the simulation, MoM (Method of Moments) is applied to generate the raw data. The MoM is a full wave simulation method and its result carries multi-path and high-order scattering, which can reflect the nature scatter characteristics. The simulation scenario is shown in Figure 2, where the blue points indicate the locations of scatters, which are sparse according to the whole scene.

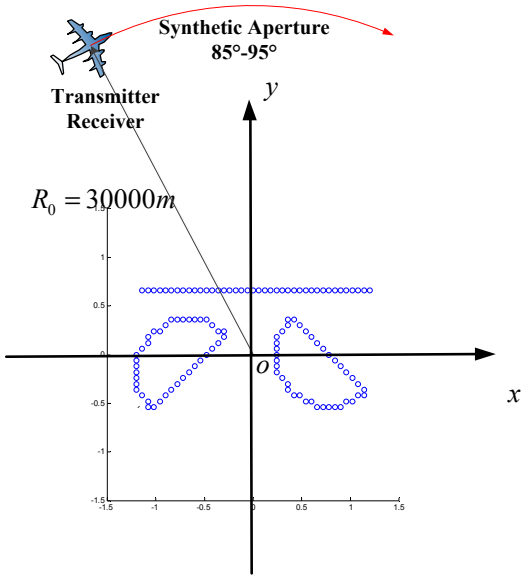

Figure 2. Simulation scenario and the radar measurement.

The aim of the simulation is to analyze the reconstruction quality and the computation time among three SAR imaging algorithms: the matched filter method, the SMV-OMP method and the MMV-OMP method. Based on the previous analyses of the imaging method, we first compare the range compression step.

(1) Range compression image

The range compression image is the foundation of a SAR image. The MF methods recover the range direction information with limited bandwidth, resulting in PSF and side-lobes. However, the CS-based methods obtain super resolution image. As for the MMV model, the image with both super resolution and lower computation cost is generated. The SMV-OMP and MMV-OMP is done with the same date rate. The structure information is applied in MMV, i.e., scatter points do not have range migration in 1° azimuth angle range. The value of L changes in different situations and is related to the initial distance and the velocity of the radar. Figure 3 shows three range compression images in different methods. The synthetic aperture angle from 85° to 95° is considered because the radar can get the specular scatting of the picture and the image is readable during the angles. Because the results of CS-based methods are sparse and most values are zero, Figure 3b,c are both discrete images. Figure 3b is punctiform, while Figure 3c is streaky.

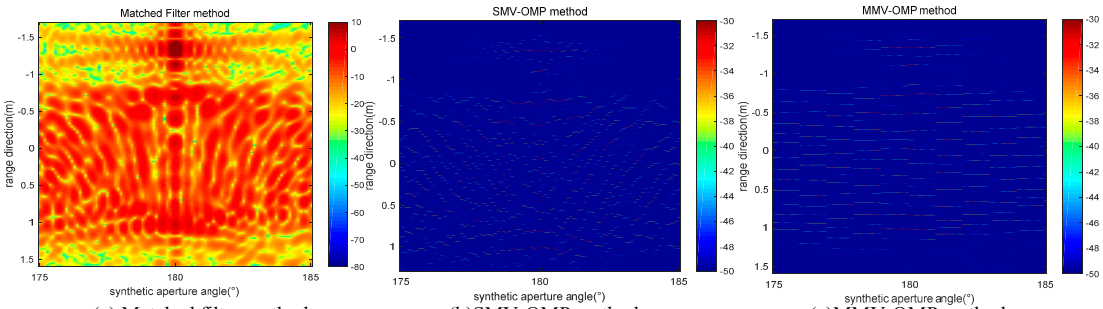

(a) Matched filter method (b)SMV-OMP method (c)MMV-OMP method

Figure 3. Recovered results: (**a**) range image with matched filter method; (**b**) range image with SMV-OMP method; and (**c**) range image with MMV-OMP method.

Both SMV and MMV method can generate super-resolution range image. The range profile with three methods in a same aperture is in Figure 4, where all methods can describe the location information in range direction and CS-based methods have the super resolution.

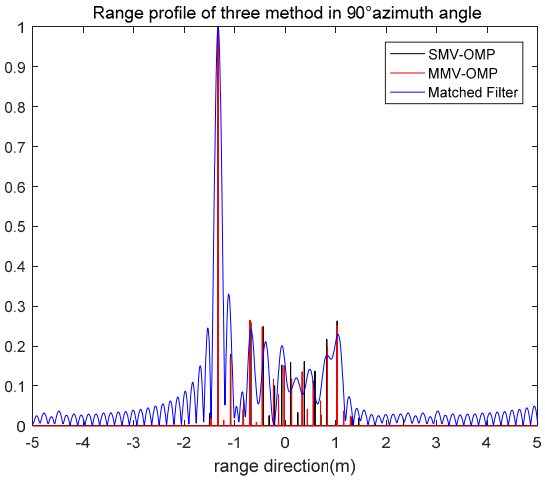

Figure 4. Range profile of three method in 90° azimuth angle.

As for the computation speed, the fastest one is the matched filter method because it does not need to compute the inversion of matrixes. Within CS methods, the MMV-OMP is faster than the SMV-OMP. The computation times of two CS methods are compared through simulation experiments. The times in different synthetic aperture angles for MMV and SMV are shown in Figure 5. The simulation is conducted in a workstation with Intel Xeon E5 CPU, 256 G RAM and Matlab 2013a.

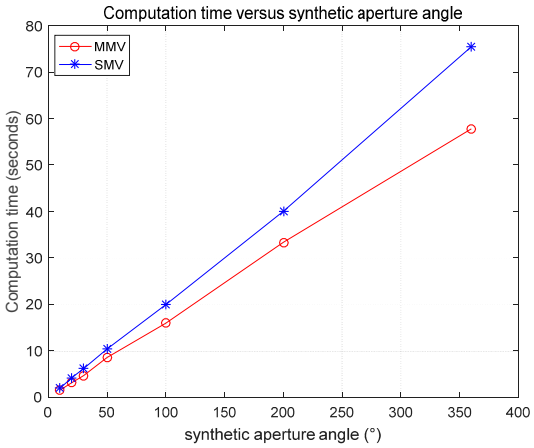

Figure 5. Computation time versus synthetic aperture angle.

When the synthetic aperture angle is small, the bias of the computing time is not obvious. However, once the data amount becomes large, the difference in the operation time becomes noticeable. For example, as for the whole 360° angle, the SMV costs 75.45 s while the MMV only 57.76 s. It is concluded the MMV model is a fast CS method.

Generally, compressed sensing is susceptible to noise. The result of random sampling is to add noise to the sparse transform domain [25]. When the sampling decreases, the corresponding noise is also greater, resulting in the more difficult to restore results. If the collected signal itself has noise, the superposition of two noise sources makes the problem difficult to solve. As a result, CS technology is typically applied only for signals with high SNR. The influence of SNR on the proposed methods is analyzed through the simulations.

In order to highlight the effects of noise, the complete data are used. The results without noise have been taken as the standard value, and we have got the RMSE performances in different SNR for SMV and MMV. Then, additional Gaussian white noise is used. The result is shown in Figure 6.

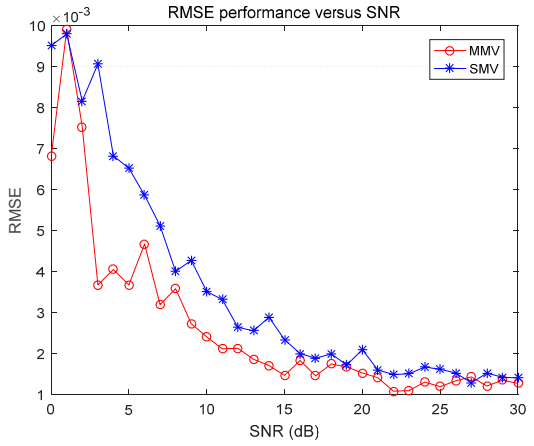

Figure 6. RMSE (Root Mean Square Error) performance of range direction result versus SNR for MMV and SMV.

As can be seen from Figure 6, the MMV model is less affected by noise. In the same SNR condition, the RMSE of MMV is smaller than SMV. Due to the structure features, more data are used and the noise is averaged during the recovery of MMV model. Thus, the MMV model performs better than the traditional sparse approach under the noise condition.

CS methods can use fewer data that are randomly sampled [34]. Thus, the data amount can also affect the recovery result. To compare the recover performance for MMV and SMV with different data amount, an experiment with different data amount has been conducted. The full data collected in an original way are set as 100 percent. One hundred Monte Carlo simulations are conducted, and their average values are regarded as results (Figure 7).

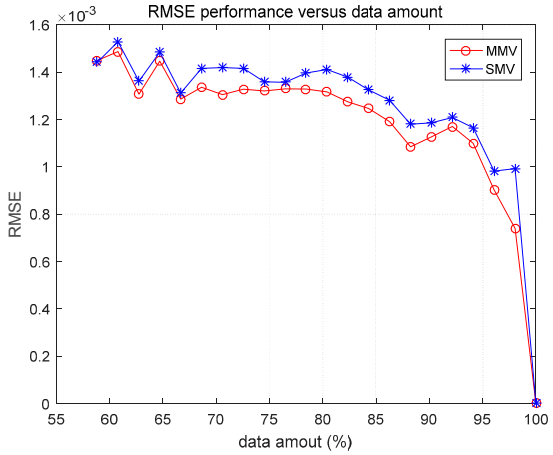

Figure 7. RMSE performance of range direction result versus date amount for MMV and SMV.

It is evident to see that the MMV model has smaller RMSE than the SMV model in Figure 6. Thus, we can say that multiple azimuth direction samples can be recovered at one time with fewer data due to the application of the MMV model.

(2) Two-Dimensional SAR imaging based on BP method

Because CS-based methods only generate the scatter parameters, we should use them to produce a continuous pattern like the MF method, which makes the azimuth processing more robust. Figure 8 is the compensated range image of CS-based methods.

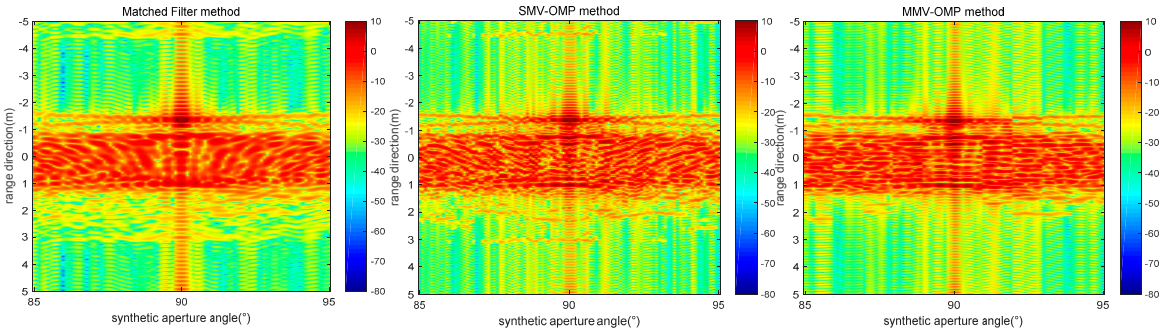

(a) Matched filter method (b)SMV-OMP method (c)MMV-OMP method

Figure 8. Compensated range image: (**a**) matched filter method; (**b**) SMV-OMP method; and (**c**) MMV-OMP method.

In Figure 8, the CS-based methods have higher resolution. However, it is only a qualitative description. A quantitative analysis of the side-lobes effects on images is shown in Figure 9. The image is the range profiles for a point target.

As can be seen from the above picture, the CS-based method images have higher resolutions than the BP. Because the compensation is the same, there is no difference between MMV and SMV in this condition. Three parameters, PSLR (Peak Side Lobe Ratio), ISLR (Integrated Side Lobe Ratio) and main lobe width, are shown in Table 2 to compare the three results quantitatively.

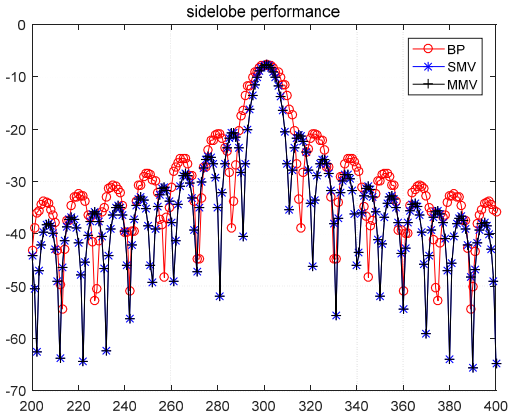

Figure 9. Side-lobe performance of three methods.

Table 2. Side-lobe performances.

	BP	SMV	MMV
PSLR (dB)	13.2474	13.3782	13.3782
ISLR (dB)	9.8874	9.9592	9.9592
main lobe width (m)	0.09	0.05	0.05

The improvement of CS-based method is due to the compensation of $\mathbf{\Phi}_{full}$. When the bandwidth of $\mathbf{\Phi}_{full}$ is higher, the performances in the three indictors are better. However, larger $\mathbf{\Phi}_{full}$ are not always better. As we discussed in Section 3.3, a $\mathbf{\Phi}_{full}$ that contains 1.5 times more frequency atoms than the original has proven to be the best choice. Here, $\mathbf{\Phi}_{full}$ with different bandwidth are shown in Figure 10.

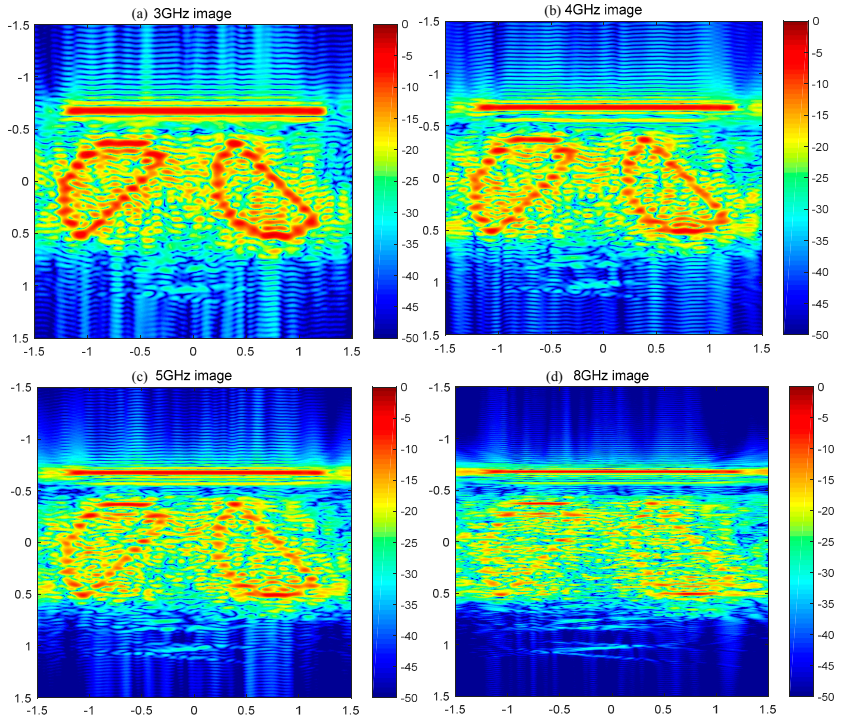

Figure 10. 2-D SAR images with different bandwidth: (**a**) 3 GHz; (**b**) 4 GHz; (**c**) 5 GHz; and (**d**) 8 GHz.

The original bandwidth is 2 GHz, and is compared to images at 3 GHz, 4 GHz, 5 GHz and 8 GHz. Many targets in the wide bandwidth images defocused or disappeared. If the original bandwidth is used, there is no benefit for the proposed method. Thus, the 1.5 times bandwidth is determined to make the image in high resolution and display the real targets better.

Figure 11 shows the final 2-D SAR images from three methods. The BP image is continuous while the two others are point-like. In reality, the scatters are located separated. Only in Figure 11b,c, can the isolated points be distinguished. It is seen that CS-based method can recovery most accurate scene information.

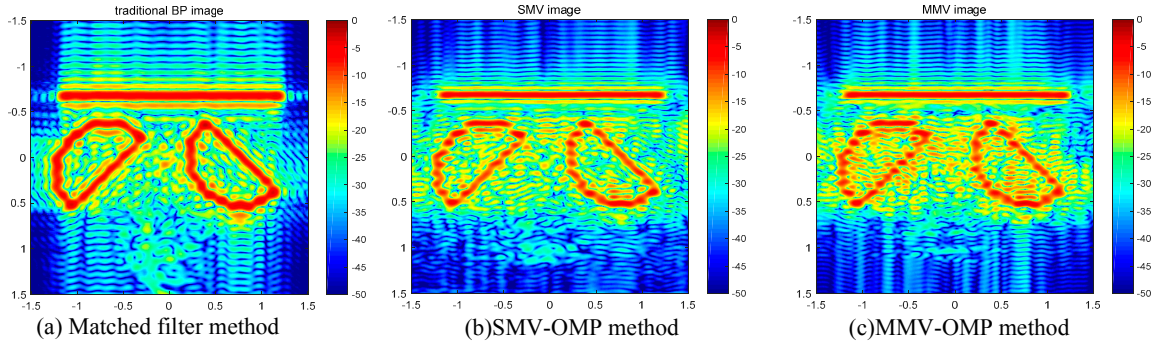

(a) Matched filter method (b)SMV-OMP method (c)MMV-OMP method

Figure 11. 2-D image of the simulation: (**a**) matched filter method; (**b**) SMV-OMP method; and (**c**) MMV-OMP method.

4.2. Regular Sparse Imaging and Improved Sparse Imaging Based on MMV

In this section, the traditional BP method, the SMV based method and the MMV based method have been applied to some real SAR imaging tasks. All experiments are conducted in the microwave anechoic chamber, and the Vector Network Analyzer is used to send and receive the stepped frequency radar signal. The experimental scenario and deceives are shown in Figure 12. A Ku antenna is applied and metal targets are set up in a rotary table, which ensures the movement of targets generates circular synthetic aperture. The SAR system parameters are listed in Table 3.

The signal model of the Vector Network Analyzer is stepped frequency. For each frequency point, the analyzer can obtain the S-parameters of the scene. By combining the data from each frequency bin, the signals detected by the radar in each PRT can be obtained, and the IFFT result is a one-dimensional range direction image.

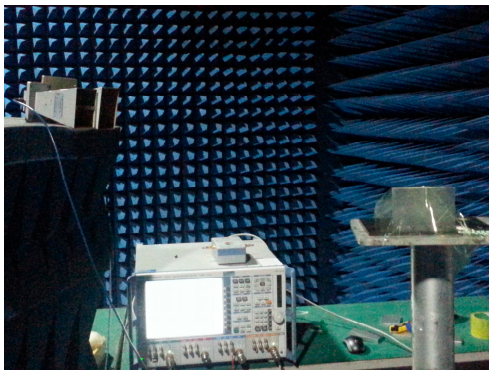

Figure 12. Experimental scenario and deceives.

Table 3. Experiment parameters.

Carrier Frequency	15 GHz
Bandwidth	6 GHz
Frequency interval	15 MHz
Angle Range	1° ~360°
Angle interval	1°
Initial Distance	0.91 m
Antenna Gain	10 dB
Antenna frequency	12–28 GHz
Antenna beamwidth	10°

According to the range of the microwave anechoic chamber and the size of the metal targets, it is assumed that the text scene is sparse. The data are proposed using three methods, and the sparsity K is set to 5. The final SAR images are processed by a reconstructive signal at 9 GHz (1.5 times the original one) bandwidth. The sampling data contain about 80% of the original data, which is the limitation specifically for the CS algorithms to examine their imaging capabilities. Three experiments with different targets, an empty scene, a circular cone and a corner reflector, are conducted. Their real image and experimental results are shown below.

The scenario of the empty scene is shown in Figure 13, where the scene is the rotary table itself, consisting of two square panels, and there is a little metal point fixed on the upper panel. The 1-D range images using different methods are shown in Figure 14.

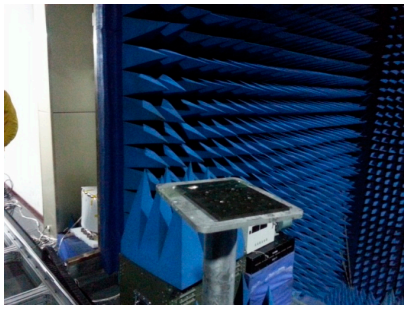

Figure 13. Experiment scenario 1.

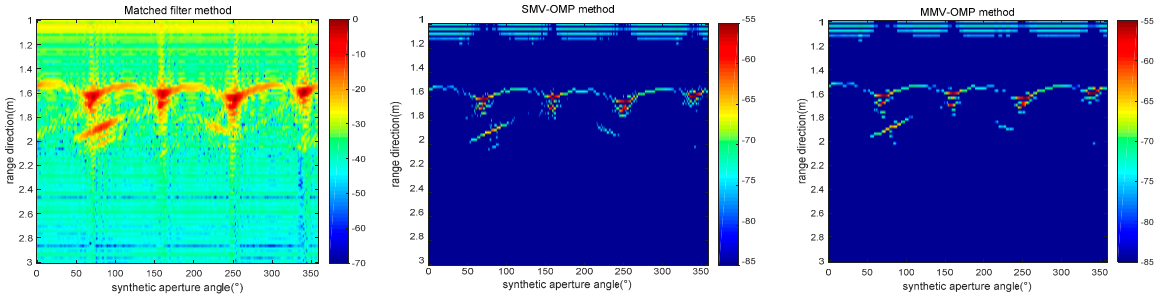

(a) Matched filter method (b)SMV-OMP method (c)MMV-OMP method

Figure 14. 1-D image of scenario 1: (**a**) matched filter method; (**b**) SMV-OMP method; and (**c**) MMV-OMP method.

The results of CS-based methods are sparse images. It is verified that the CS images have the essential features of the empty scene when compared with Figure 12a. Specular scatting phenomena occur in the same place with the matched filter method. After azimuth processing, their final imaging results are shown in Figure 15.

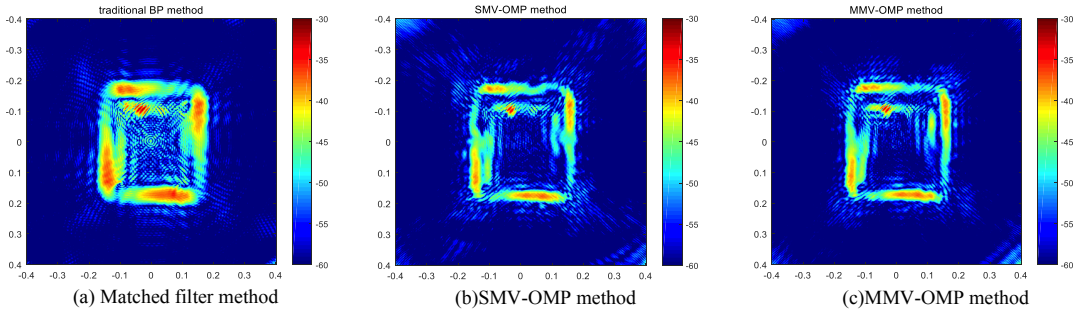

Figure 15. 2-D image of scenario 1: (**a**) matched filter method; (**b**) SMV-OMP method; and (**c**) MMV-OMP method.

The image improvements of Figure 15b,c are that the strong point on the inner plane becomes more distinguished and the space between the big and the small plane is larger than the matched filter one. Besides, the outline of the table in Figure 15c is the clearest.

The scenario of experiment 2 is shown in Figure 16. A circular cone is added to the scenario of experiment 1.

Figure 16. Experiment scenario 2.

The 1-D range image result of scenario 2 is shown in Figure 17.

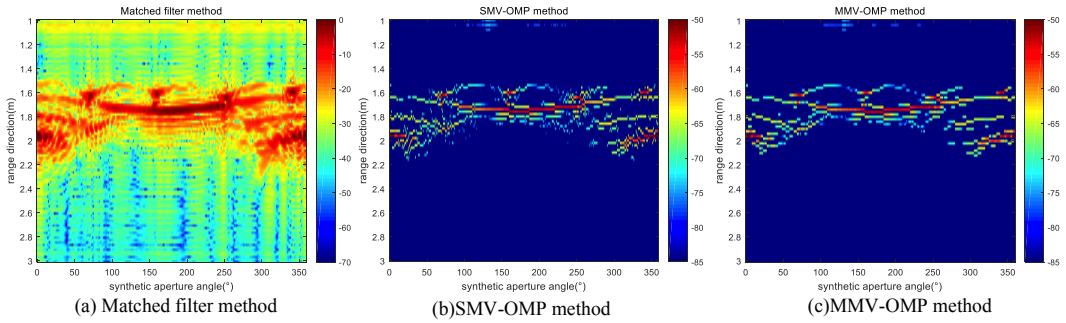

Figure 17. 1-D image of scenario 2: (**a**) matched filter method; (**b**) SMV-OMP method; and (**c**) MMV-OMP method.

As can be seen from Figure 17, the difference between MMV and SMV is that the MMV model has more fake targets than the SMV. Because it is assumed that the range images have the same location information in a range of azimuth apertures, these fake targets will disappear in the final SAR image where only the targets with value in all proper apertures maintain. The final 2-D SAR images are shown in Figure 18.

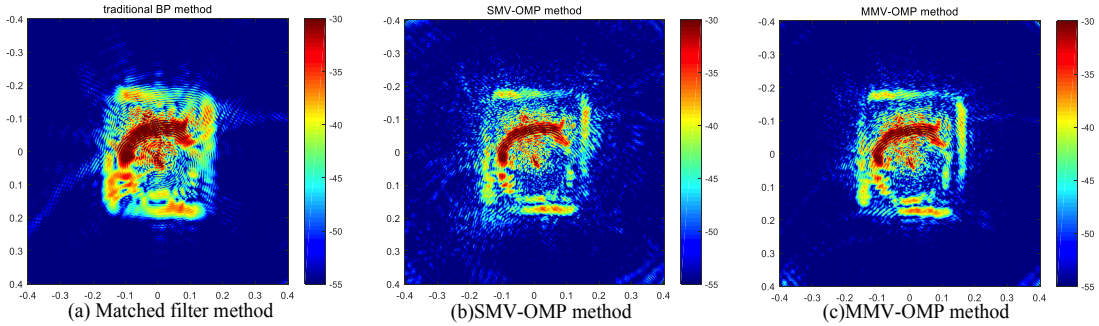

Figure 18. 2-D image of scenario 2: (**a**) matched filter method; (**b**) SMV-OMP method; and (**c**) MMV-OMP method.

The images based on CS theory in Figure 16 are clearer and the circle of the target is more obvious. Meanwhile, the side-lobes of the targets in Figure 18c are less than those in Figure 18b, especially in the outside of the rotating table. It is verified that the MMV based image algorithm is efficient and effective.

Finally, the most common target in radar imaging, corner reflector, has been tested in the experiment shown in Figure 19.

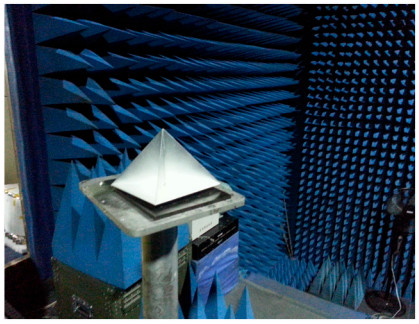

Figure 19. Experiment scenario 3.

Because the high radar cross section of a corner reflector exists in wide aperture range, all 1-D images occur as a red light line, as shown in Figure 20.

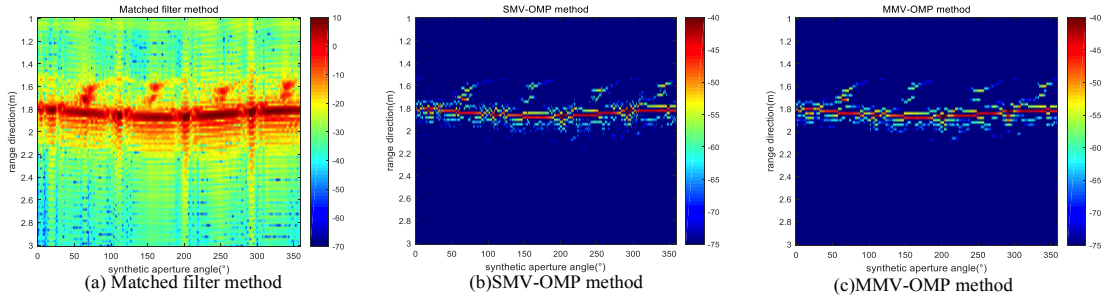

Figure 20. 1-D image of scenario 3: (**a**) matched filter method; (**b**) SMV-OMP method; and (**c**) MMV-OMP method.

The 2-D images are shown in Figure 21. The corner reflector is clearly recognized in all three images. As for the CS-based images, the boundary of the corner reflector is more distinct.

Compared with the BP algorithm, the improved CS method has higher resolution and can reconstruct the actual targets better. The real data experiments support that the combination of CS

theory and traditional SAR image method is a new way to generate SAR images, especially applicable to high-resolution SAR imaging applications.

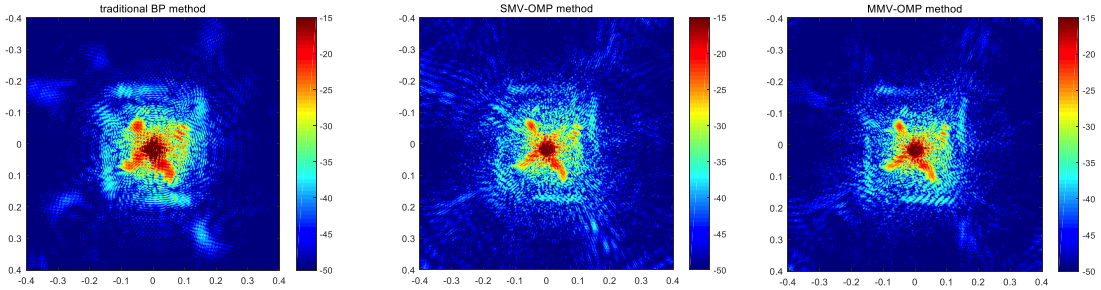

Figure 21. 2-D image of scenario 3: (**a**) matched filter method; (**b**) SMV-OMP method; and (**c**) MMV-OMP method.

5. Discussion

The proposed MMV-based SAR imaging method generates super-resolution images with high image quality and fast speed. In both simulations and experiments, the performance of the MMV method is the best. Besides, the algorithm has simple structure and is easy to implement. The main reason for the improvement is that both the CS method and the traditional imaging method are applied. In the range direction, the CS method is used to obtain the super-resolution range. In the azimuth direction, the traditional matched filter method guarantees the robustness of the SAR images. Combining the advantages of two methods, the proposed MMV method performances particularly well in both the image quality and the operational efficiency.

Compared with the conventional CS-based method, a 2-D decoupled processing flow is built for SAR imaging, which makes the algorithm more practical and robust. Unsupervised algorithms require the vectorization of images, which results in both processing efficiency and the imaging scene scope being constrained by the computing conditions. Compared with traditional BP method, MMV technology can effectively enhance the resolution of the image, while reducing the demand for data.

In this paper, the basic principle of SAR imaging is studied deeply, and the CS technology is specifically optimized to broaden its applications. Meanwhile, it has opened up an entirely new way of super-resolution SAR imaging. This article also has some shortcomings, such as the requirement of sparse scenes and the restrictions on system architecture. However, it is believed that this SAR processing system with a variety of advantages can be widely applied.

6. Conclusions

In this paper, a novel method based on the MMV model has been used to generate high-quality SAR images in a stepped frequency circular SAR system. If the targets are sparse or compressible, an exact reconstruction can be achieved with high resolution and low computation time. Based on the theory of radar imaging, the traditional SAR imaging method is summarized. In order to overcome the limitations of traditional methods, the application of CS theory in microwave radar imaging is discussed and its background is analyzed. However, the conventional CS imaging algorithms have large computing burden and are short of the optimization for SAR imaging. Usually, they are complex and only work in small-scale scenes. In this paper, the MMV based CS imaging method is proposed, which introduces the modern signal processing technique into the traditional signal processing field. The new algorithm has advantages in computation and stability. The available imaging scenes will be extended significantly, while the range and azimuth resolutions are maintained. Both the simulation and experimental results have shown the validity and advantages of the proposed imaging scheme.

Future works will include fast reconstruction strategies and detailed investigations of the sparsity and compressibility of the targets. Sparsity is a necessary condition for the application of the CS

theory. However, in some situations, speckle noise will make the phase of the reflectivity map random. Thus, it is difficult to find an efficient sparse transform for a complex reflectivity map. In this case, the effective signal model of targets should be investigated to make the inversion of SAR signal more precise.

Acknowledgments: This work is supported by National Natural Science Foundation of China (Grant No. 61120106004, 61427802, and 61225005), Beijing Natural Science Foundation (Grant No. 4162052), Chang Jiang Scholars Program (T2012122), 111 project of China under Grant B14010, and China Scholarship Council (CSC).

Author Contributions: Dongyang Ao and Cheng Hu conceived and designed the experiments; Dongyang Ao, Rui Wang and Yuanhao Li performed the experiments; Rui Wang and Cheng Hu contributed the experimental equipment; Dongyang Ao wrote the paper; Yuanhao Li revised the English.

Conflicts of Interest: The authors declare no conflict of interest.

References

1. Curlander, J.C.; McDonough, R.N. *Synthetic Aperture Radar*; John Wiley & Sons: New York, NY, USA, 1991.
2. Yu, Z.; Wang, S.; Li, Z. An Imaging Compensation Algorithm for Spaceborne High-Resolution SAR Based on a Continuous Tangent Motion Model. *Remote Sens.* **2016**, *8*, 223. [CrossRef]
3. Garzelli, A. A Review of Image Fusion Algorithms Based on the Super-Resolution Paradigm. *Remote Sens.* **2016**, *8*, 797. [CrossRef]
4. Baraniuk, R.G.; Steeghs, P. Compressive radar imaging. In Proceedings of the IEEE Radar Conference, Boston, MA, USA, 17–20 April 2007; pp. 128–133.
5. Patel, V.M.; Easley, G.R.; Healy, D.M., Jr.; Chellappa, R. Compressed synthetic aperture radar. *IEEE J. Sel. Top. Signal Process.* **2010**, *4*, 244–254. [CrossRef]
6. Alonso, M.T.; López-Dekker, P.; Mallorquí, J.J. A novel strategy for radar imaging based on compressive sensing. *IEEE Trans. Geosci. Remote Sens.* **2010**, *48*, 4285–4295. [CrossRef]
7. Zhu, X.X.; Bamler, R. Tomographic SAR inversion by L1-norm regularization—The compressive sensing approach. *IEEE Trans. Geosci. Remote Sens.* **2010**, *48*, 3839–3846. [CrossRef]
8. Zhu, X.X.; Bamler, R. Super-resolution power and robustness of compressive sensing for spectral estimation with application to spaceborne tomographic SAR. *IEEE Trans. Geosci. Remote Sens.* **2012**, *50*, 247–258. [CrossRef]
9. Bu, H.; Tao, R.; Bai, X.; Zhao, J. A Novel SAR Imaging Algorithm Based on Compressed Sensing. *IEEE Geosci. Remote Sens. Lett.* **2015**, *12*, 1003–1007.
10. Shen, F.; Zhao, G.; Shi, G.; Dong, W.; Wang, C.; Niu, Y. Compressive SAR Imaging with Joint Sparsity and Local Similarity Exploitation. *Sensors* **2015**, *15*, 4176–4192. [CrossRef] [PubMed]
11. Xiao, P.; Yu, Z.; Li, C. Compressive sensing SAR range compression with chirp scaling principle. *Sci. China Inf. Sci.* **2012**, *55*, 2292–2300. [CrossRef]
12. Massa, A.; Rocca, P.; Oliveri, G. Compressive Sensing in Electromagnetics—A Review. *IEEE Antennas Propag. Mag.* **2015**, *57*, 224–238. [CrossRef]
13. Phillips, J.W.; Leahy, R.M.; Mosher, J.C. MEG-based imaging of focal neuronal current sources. *IEEE Trans. Med. Imaging* **1997**, *16*, 338–348. [CrossRef] [PubMed]
14. Gribonval, R. Sparse decomposition of stereo signals with matching pursuit and application to blind separation of more than two sources from a stereo mixture. In Proceedings of the IEEE International Conference Acoustics, Speech, Signal Processing (ICASSP), Minneapolis, MN, USA, 27–30 April 1993.
15. Malioutov, D.; Cetin, M.; Willsky, A.S. A sparse signal reconstruction perspective for source localization with sensor arrays. *IEEE Trans. Signal Process.* **2005**, *53*, 3010–3022. [CrossRef]
16. Hyder, M.M.; Mahata, K. A robust algorithm for joint-sparse recovery. *IEEE Signal Process. Lett.* **2009**, *16*, 1091–1094. [CrossRef]
17. Méndez-Rial, R.; Rusu, C.; Alkhateeb, A.; González-Prelcic, N.; Heath, R.W. Channel estimation and hybrid combining for mmwave: Phase shifters or switches? In Proceedings of the Information Theory and Applications Workshop (ITA), San Diego, CA, USA, 1–6 February 2015; pp. 90–97.
18. Li, Y.; Chi, Y. Off-the-grid line spectrum denoising and estimation with multiple measurement vectors. *IEEE Trans. Signal Process.* **2016**, *64*, 1257–1269. [CrossRef]

19. Sharma, S.K.; Lagunas, E.; Chatzinotas, S.; Ottersten, B. Application of compressive sensing in cognitive radio communications: A survey. *IEEE Commun. Surv. Tutor.* **2016**, *99*, 1–24. [CrossRef]
20. Oriot, H.; Cantalloube, H. Circular SAR imagery for urban remote sensing. In Proceedings of the 7th European Conference on Synthetic Aperture Radar (EUSAR), Friedrichshafen, Germany, 2–5 June 2008; pp. 1–4.
21. Li, B.; Liu, F.; Zhou, C.; Lv, Y.; Hu, J. Fast compressed sensing SAR imaging using stepped frequency waveform. In Proceedings of the 2016 IEEE International Conference on Microwave and Millimeter Wave Technology (ICMMT), Beijing, China, 5–8 June 2016; pp. 521–523.
22. Chen, J.; Zeng, T.; Long, T. A novel high-resolution stepped frequency SAR signal processing method. In Proceedings of the IET International Radar Conference, Guilin, China, 20–22 April 2009; pp. 1–4.
23. Yang, J.; Huang, X.; Jin, T.; Thompson, J.; Zhou, Z. Synthetic aperture radar imaging using stepped frequency waveform. *IEEE Trans. Geosci. Remote Sens.* **2012**, *50*, 2026–2036. [CrossRef]
24. Shkvarko, Y.V.; Yañez, J.I.; Amao, J.A.; del Campo, G.D.M. Radar/SAR Image Resolution Enhancement via Unifying Descriptive Experiment Design Regularization and Wavelet-Domain Processing. *IEEE Geosci. Remote Sens. Lett.* **2016**, *13*, 152–156. [CrossRef]
25. Duarte, M.F.; Eldar, Y.C. Structured compressed sensing: From theory to applications. *IEEE Trans. Signal Process.* **2011**, *59*, 4053–4085. [CrossRef]
26. Rauhut, H. Compressive Sensing and Structured Random Matrices. In *Theoretical Foundations and Numerical Methods for Sparse Recovery*; Fornasier, M., Ed.; deGruyter: Goetingen, Germany, 2010; Volume 9, pp. 1–92.
27. Tropp, J.A.; Laska, J.N.; Duarte, M.F.; Romberg, J.K.; Baraniuk, R.G. Beyond Nyquist: Efficient Sampling of Sparse Bandlimited Signals. *IEEE Trans. Inf. Theory* **2010**, *56*, 520–544. [CrossRef]
28. Baron, D.; Wakin, M.B.; Duarte, M.F.; Sarvotham, S.; Baraniuk, R.G. Distributed compressed sensing. *IEEE Trans. Inf. Theory* **2006**, *52*, 5406–5425.
29. Davies, M.E.; Eldar, Y.C. Rank awareness in joint sparse recovery. *IEEE Trans. Inf. Theory* **2012**, *58*, 1135–1146. [CrossRef]
30. Mishali, M.; Eldar, Y.C. Reduce and boost: Recovering arbitrary sets of jointly sparse vectors. *IEEE Trans. Signal Process.* **2008**, *56*, 4692–4702. [CrossRef]
31. Leviatan, D.; Temlyakov, V.N. Simultaneous approximation by greedy algorithms. *Adv. Comput. Math.* **2006**, *25*, 73–90. [CrossRef]
32. Tropp, J.A.; Gilbert, A.C.; Strauss, M.J. Algorithms for simultaneous sparse approximation. Part I: Greedy pursuit. *Signal Process.* **2006**, *86*, 572–588. [CrossRef]
33. Blanchard, J.D.; Cermak, M.; Hanle, D.; Jing, Y. Greedy Algorithms for Joint Sparse Recovery. *IEEE Trans. Signal Process.* **2014**, *62*, 1694–1704. [CrossRef]
34. Gorodnitsky, I.F.; Rao, B.D. Sparse signal reconstruction from limited data using FOCUSS: A re-weighted minimum norm algorithm. *IEEE Trans. Signal Process.* **1997**, *45*, 600–616. [CrossRef]
35. Chen, S.S.; Donoho, D.L.; Saunders, M.A. Atomic decomposition by basis pursuit. *SIAM J. Sci. Comput.* **1998**, *20*, 33–61. [CrossRef]
36. Song, S.; Xu, B.; Yang, J. SAR Target Recognition via Supervised Discriminative Dictionary Learning and Sparse Representation of the SAR-HOG Feature. *Remote Sens.* **2016**, *8*, 683. [CrossRef]
37. Pati, Y.C.; Rezaiifar, R.; Krishnaprasad, P. Orthogonal matching pursuit: Recursive function approximation with applications to wavelet decomposition. In Proceedings of the Twenty-Seventh Asilomar Conference on Signals, Systems and Computers, Pacific Grove, CA, USA, 1–3 November 1993; pp. 40–44.
38. Gribonval, R.; Rauhut, H.; Schnass, K.; Vandergheynst, P. Atoms of all channels, unite! Average case analysis of multi-channel sparse recovery using greedy algorithms. *J. Fourier Anal. Appl.* **2008**, *14*, 655–687. [CrossRef]